Int J Earth Sciences (Geol Rundsch) (2001) 90:28–45
DOI 10.1007/s005310000149

ORIGINAL PAPER

J.H.P. De Bresser · J.H. Ter Heege · C.J. Spiers

Grain size reduction by dynamic recrystallization: can it result in major rheological weakening?

Received: 22 September 1999 / Accepted: 9 October 2000 / Published online: 20 December 2000

Abstract It is widely believed that grain size reduction by dynamic recrystallization can lead to major rheological weakening and associated strain localization by bringing about a switch from grain size insensitive dislocation creep to grain size sensitive diffusion creep. Recently, however, we advanced the hypothesis that, rather than a switch, dynamic recrystallization leads to a balance between grain size reduction and grain growth processes set up in the neighborhood of the boundary between the dislocation creep field and the diffusion creep field. In this paper, we compare the predictions implied by our hypothesis with those of other models for dynamic recrystallization. We also evaluate the full range of models against experimental data on a variety of materials. We conclude that a temperature dependence of the relationship between recrystallized grain size and flow stress cannot be neglected a priori. This should be taken into account when estimating natural flow stresses using experimentally calibrated recrystallized grain size piezometers. We also demonstrate experimental support for the field boundary hypothesis. This support implies that significant weakening by grain size reduction in localized shear zones is possible only if caused by a process other than dynamic recrystallization (such as syntectonic reaction or cataclasis) or if grain growth is inhibited.

Keywords Deformation · Microstructures · Paleopiezometry · Rheology · Recrystallization

J.H.P. De Bresser (✉) · J.H. Ter Heege · C.J. Spiers
HPT-Laboratory, Faculty of Earth Sciences, Utrecht University, P.O. Box 80.021, 3508 TA Utrecht, The Netherlands
E-mail: j.h.p.debresser@geo.uu.nl
Phone: +31-30-2534973
Fax: +31-30-2537725

Introduction

The localization of strain in deforming rocks is believed to be of prime importance in controlling the dynamics of the lithosphere. Commonly, localized deformation zones show a grain size that is reduced with respect to that in the protolith (e.g. White et al. 1980; Tullis and Yund 1985; Jin et al. 1998; Shigematsu 1999). Associated with this reduction in grain size, a general rheological weakening is inferred (Poirier 1980; Hobbs et al. 1990). Meaningful modeling of deformation behavior of rocks must therefore include the rheological changes linked with grain refinement and localization, as emphasized in work by, amongst others, Furlong (1993), Govers and Wortel (1995) and Braun et al. (1999).

Several different mechanisms can result in grain size reduction during deformation. These include cataclasis (e.g., Hippler and Knipe 1990), syntectonic, metamorphic reaction (e.g., Newman et al. 1999), and dynamic recrystallization during recovery-controlled creep (e.g., Tullis et al. 1990; Hirth and Tullis 1992). The last of these mechanisms is of particular interest because experimental work on numerous metals, ceramics, and rocks has demonstrated that the mean recrystallized grain diameter D (usually referred to as the "grain size") can be related to the steady state flow stress σ by an equation of the type

$$D = K\sigma^{-m} \quad (1)$$

where K and m (typically 0.7–1.6) are material- and mechanism-specific constants (Takeuchi and Argon 1976; Twiss 1977; Drury et al. 1985; Rutter 1995). If calibrated experimentally, this type of D–σ relation can be used to estimate paleo-stresses from the microstructure of naturally deformed rocks (White 1979), providing a useful tool in quantifying lithosphere dynamics. In addition, D–σ relations obtained for geological materials such as olivine and calcite have been

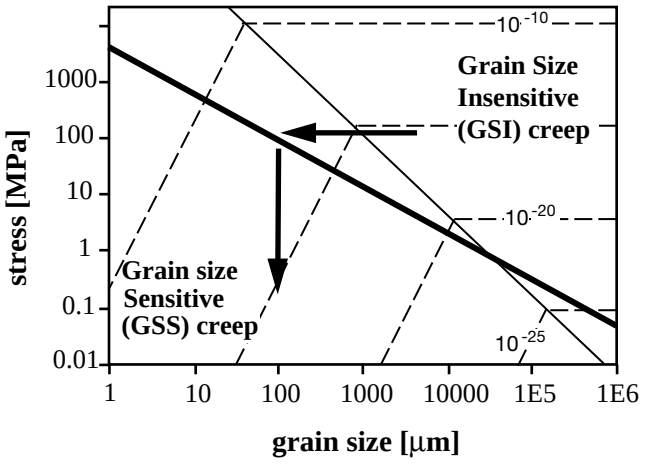

Fig. 1 Empirical stress versus recrystallized grain size relation (*heavy line*) for olivine extrapolated into a deformation mechanism map drawn for a temperature of 600 °C. Based on data from Rutter and Brodie (1988). Strain rate contours in s^{-1}. The *arrows* illustrate the notion of rheological weakening resulting from a switch in deformation mechanism associated with grain size reduction by dynamic recrystallization, at constant strain rate

extrapolated into deformation mechanism maps plotted using mechanical data from the laboratory (e.g., Schmid 1982; Karato et al. 1986; Handy 1989; Jaroslow et al. 1996). Such D–σ relations often transect the boundary between the dislocation and diffusion creep fields (Fig. 1). On this basis, it has been proposed that grain size reduction by dynamic recrystallization can bring about a switch from grain size insensitive (GSI) dislocation creep to grain size sensitive (GSS) diffusion creep (Schmid 1982; Rutter and Brodie 1988; Furlong 1993; Busch and Van der Pluijm 1995; Vissers et al. 1995). These two mechanisms act as parallel-concurrent processes, hence the fastest controls creep (Poirier 1985). A switch to GSS creep would thus result in significant rheological weakening, with flow stresses potentially decreasing more than an order of magnitude in the case of olivine deformed at constant (geological) strain rate (see Fig. 1).

Recently, we argued that a clear-cut switch in deformation mechanism from GSI to GSS creep is unlikely to occur in single phase materials (De Bresser et al. 1998) because new grains produced by dynamic recrystallization in the GSI field may initially be sufficiently small to deform by GSS mechanisms, but will subsequently grow until dislocation processes become significant again. We advanced the hypothesis that dynamic recrystallization may accordingly represent a balance between grain size reduction and grain growth processes set up in the boundary region between the dislocation creep field and the diffusion creep field. Results of creep experiments on a metallic rock analogue, Magnox Al80, demonstrated a D–σ relation in good agreement with this "field boundary hypothesis".

The aim of the present follow-up paper is twofold. First, we will briefly review previous microphysical models addressing the relationship between recrystallized grain size and flow stress [Eq. (1)], and we will compare these models with our field boundary hypothesis. Second, we will evaluate the various models and field boundary hypothesis by comparison with experimental data for a number of materials. It will be shown that existing recrystallized grain size versus stress data, in particular for olivine and calcite, lend support to the suggested balance at the GSI–GSS field boundary, implying that major weakening in localized natural deformation zones cannot be caused by dynamic recrystallization, unless grain growth is inhibited.

Models for recrystallization during recovery-controlled creep

In broad terms, two end-member mechanisms of dynamic recrystallization can be distinguished (e.g., Guillopé and Poirier 1979; Urai et al. 1986; Drury and Urai 1990): (1) rotation recrystallization and (2) migration recrystallization. The first mechanism involves the formation of new, high angle grain boundaries from subgrain boundaries, either by progressive misorientation of subgrains or by sub-boundary migration and coalescence in areas of high lattice curvature. New grains developed by rotation mechanisms may subsequently grow. In migration recrystallization, existing grain boundaries migrate, and a reworked microstructure develops because of grain dissection, grain coalescence and development of new grains from grain boundary bulges (e.g., Means 1989). Dynamic recrystallization in real materials generally involves components of both end members.

Few quantitative microphysical models exist to underpin the above mechanisms of recrystallization, their interaction or the observed relation between recrystallized grain size and flow stress at steady state. Probably the most widely quoted model is that of Twiss (1977), who derived relationships between both subgrain size and stress, and recrystallized grain size and stress. No explicit distinction was made by Twiss between rotation and migration mechanisms. In contrast, the model presented by Derby and Ashby (1987) specifically concentrates on migration recrystallization, with new grain "nucleation" occurring by grain boundary bulging. Recent work by Shimizu (1998) describes the development and growth of new grains formed by progressive subgrain rotation. These models for dynamic recrystallization and the resulting D–σ relationships will be briefly discussed below, as will our boundary hypothesis model. Because the Twiss, Derby/Ashby and Shimizu models all incorporate subgrain development as an essential element, we will also include the subgrain model of Edward et al. (1982) in our discussion.

The Twiss model

The model presented by Twiss (1977) is based on the assumption that there exists a unique (sub)grain size at which the total strain energy of dislocations ordered in a subgrain boundary or in a recrystallized grain boundary is equal to the stored energy of the dislocations in the enclosed volume. The flow stress σ is introduced into the model through the usual relationship with dislocation density $\sigma \propto \rho^{0.5}$ (Nabarro 1987). Using equations for boundary and volume energies for an idealized, cubic (sub)grain structure, with all boundaries being simple tilt walls and all dislocations being of edge type, the following equation resulted:

$$D^* = K\sigma^{-m} \text{ with } m = \left(\frac{2\phi - 1}{\phi}\right) \tag{2}$$

where D^* represents either subgrain or recrystallized grain size, K is a constant and ϕ is the ratio of total dislocation length in the (sub)boundary to that in the enclosed volume. The value of the parameter ϕ is the only difference between the subgrain and recrystallized grain size models. Twiss argues that if ϕ is smaller than 1, dislocations in the enclosed volume will increase their energy rather than decrease if moving into the boundary, hence the boundary will not form. If it is assumed that the subgrain size d_s that forms is the smallest possible stable size, ϕ must be taken as 1, yielding:

$$d_s = K_1\sigma^{-1} \tag{3}$$

Recrystallized grains are thought to develop by expansion of dislocation loops, moving outward to form grain boundaries. Only those dislocations originally present in the enclosed volume at the time of recrystallization are involved in the grain boundary formation. In that way, ϕ is minimized and the produced recrystallized grains are dislocation-free and remain so. Thus, it is assumed that the smallest stable grain size is the one that develops. Values for ϕ are estimated to be $1.4 \leq \phi \leq 2$, resulting in:

$$D = K_2\sigma^{-m} \text{ with } 1.3 \leq m \leq 1.5 \tag{4}$$

where D is the recrystallized grain size and K_2 is a constant.

The Edward model

Edward et al. (1982) present a model for the development of a steady state subgrain structure that is based on a dynamic balance between the flux of dislocations gliding and climbing into subgrain walls and the climb-controlled annihilation of dislocations at nodal points in the sub-boundary network. Accordingly, the relationship between the subgrain size d_s and flow stress σ at steady state is determined by the product of dislocation generation rate and mean slip distance (flux), and by the climb velocity in the subgrain wall. The flux term is directly related to the creep behavior of the material, whereas the nodal annihilation term embodies the diffusivity for climb in sub-boundaries. Expressing the creep behavior by a conventional power law (Dorn) equation

$$\dot{\varepsilon}_r = B\sigma^n \exp\left(\frac{-Q_r}{RT}\right) \tag{5}$$

where B and n (the "power law exponent") are constants, Q_r represents the activation energy for the process controlling the rate of dislocation creep $\dot{\varepsilon}_r$, R is the gas constant, and T is the absolute temperature, the d_s-σ relation obtained by Edward et al. is:

$$d_s = K_3\sigma^{-n/4} \exp\left(\frac{Q_r - Q_{cl}}{4RT}\right) \tag{6}$$

where K_3 is a constant and Q_{cl} is the activation energy for the diffusion process controlling dislocation climb in the boundary.

The Derby and Ashby model

Derby and Ashby (1987) and Derby (1990) present a model for dynamic recrystallization by grain boundary migration. A steady state mean grain size D is achieved by competition between grain nucleation by bulging at grain boundaries, and grain growth events. An estimate of the mean grain size D is obtained by balancing the rate of bulge nucleation with the mean boundary migration rate, reasoning that at steady state there should be one nucleation event in a volume of D^3 in the time required for a moving grain boundary to sweep out a similar volume. The driving force for both bulge nucleation and grain boundary migration is related to the energy stored in subgrain walls formed during deformation at elevated temperature. The number of nuclei (per unit area) is related to the strain of the material during one cycle of recrystallization, hence the nucleation rate is directly related to the strain rate during the cycle time. The rate of grain boundary migration depends linearly on the driving force via a mobility term that includes the boundary thickness and grain boundary diffusion coefficient. Assuming that the mean strain rate during recrystallization is the same as determined by the steady state creep behavior of the material [cf. Eq. (5), assuming creep is controlled by lattice diffusion], the following relation between D and σ results:

$$D = K_4 \exp\left(\frac{Q_v - Q_{gb}}{2RT}\right)\sigma^{-n/2} \tag{7}$$

where K_4 is a constant, Q_v and Q_{gb} are the activation energies for lattice and grain boundary diffusion, respectively, and n is again the stress exponent in the power law creep equation [Eq. (5)]. The Derby and

Ashby model critically depends on differences in subboundary spacing between neighboring grains. Note, however, that the derivation of Eq. (7) does not include use of a subgrain size-stress relation of the type of Eqs. (3) or (6).

The Shimizu model

In the model put forward by Shimizu (1998), new grains "nucleate" via progressive misorientation (rotation) of subgrains. A steady state recrystallized grain size D is formed because of a balance between the rate of nucleation and the (radial) growth rate of the newly created grains. This is similar to the foundation of the Derby and Ashby model for migration recrystallization. However, Shimizu's approach takes into account the fact that real materials undergoing recrystallization show a distribution of grain sizes rather than a single value (see also Shimizu 1999), and the characteristic grain size parameter D is accordingly defined as the maximum frequency in a logarithmic frequency diagram.

The nucleation rate in Shimizu's model depends on the number of nucleation sites (subgrains) per unit volume and the time required to develop new grain nuclei by subgrain rotation. The nuclei are assumed to be spherical and to have the same size as subgrains. The density of potential nucleation sites (subgrains) can be independently specified for intracrystalline nucleation and nucleation at grain boundaries, making use of the inverse relation between d_s and σ of Eq. (3). The time required for subgrains to become nuclei is determined by the flux of dislocations climbing into the subgrain boundaries, i.e., by the product of the free dislocation density ρ and the climb velocity of the dislocations.

The radial growth rate is assumed constant by Shimizu and depends on the grain boundary mobility, hence the grain boundary diffusion coefficient, in the same way as implemented by Derby and Ashby (1987). In order to obtain a σ–D relationship, stress is introduced through the expression $\sigma \propto \rho^{0.5}$ and the above mentioned $d_s \propto \sigma^{-1}$ relation [Eq. (3)]. The result is:

$$D = K_5 \sigma^{-1.25} \exp\left(\frac{Q_v - Q_{gb}}{4RT}\right) \quad (8)$$

for intracrystalline nucleation, and

$$D = K_6 \sigma^{-1.33} \exp\left(\frac{Q_v - Q_{gb}}{3RT}\right) \frac{Q_v - Q_{gb}}{3RT} \quad (9)$$

for grain boundary nucleation. Here, Q_v is the activation energy for lattice diffusion, which controls dislocation climb towards sub-boundaries, but not necessarily controls creep. Note that the model implies that recrystallized grains nucleated from subgrains are always larger than the original subgrains.

The field boundary hypothesis

The Derby and Ashby model for migration recrystallization as well as the Shimizu model for rotation recrystallization incorporate a dynamic balance between grain size reduction (via nucleation of new grains) and grain growth, both driven by dislocation stored energy. These models should be regarded as end-members of a range of potential combinations of the two basic recrystallization mechanisms that can accompany dislocation creep (see also Drury and Urai 1990). During dynamic recrystallization, new grains might be sufficiently small to deform by grain size sensitive mechanisms. However, grain surface energy may then become a driving force for grain boundary migration in addition to dislocation stored energy, resulting in grain growth. This reasoning was used in our earlier paper (De Bresser et al. 1998) to argue that the grain size of a dynamically recrystallizing material will tend to organize itself so that deformation proceeds in the boundary between the grain size insensitive (GSI) dislocation creep field and the grain size sensitive (GSS) diffusion creep field. The hypothesis is briefly reviewed below.

If a single phase material has a sufficiently fine starting grain size, deformation will initially be grain size sensitive. However, the grains will then grow under the action of surface energy until dislocation processes become significant. At that point, bulge nucleation and/or progressive subgrain rotation processes will produce fine new grains, re-promoting GSS flow mechanisms. Conversely, in an initially coarse material, bulge nucleation and/or rotation recrystallization accompanying dislocation (GSI) creep will lead to grain size reduction. This will promote GSS mechanisms, which will in turn be counteracted by grain growth. On this basis, we suggested in our 1998 paper that, in materials in which grain size reduction is sufficiently effective, dynamic recrystallization should lead to a steady state balance between grain size reduction and grain growth processes set up in the boundary region between the dislocation (GSI) and diffusion (GSS) creep field. The boundary can be located using the relation for dislocation creep given by Eq. (5), plus that for diffusion creep expressed:

$$\dot{\varepsilon}_d = A\left(\frac{\sigma}{d^p}\right) \exp\left(\frac{-Q_d}{RT}\right) \quad (10)$$

where A and p are constants, d is the grain size, and Q_d is the activation energy for lattice or grain boundary diffusion (i.e., Q_v and p=2, or Q_{gb} and p=3, respectively). Near the boundary, both dislocation and diffusion creep will contribute to the overall steady state creep rate $\dot{\varepsilon}_{rx}$. Because the mechanisms are parallel-concurrent, their strain rates are additive, so that

$$\dot{\varepsilon}_{rx} = \dot{\varepsilon}_d + \dot{\varepsilon}_r \quad (11)$$

At the boundary both mechanisms contribute equally to the overall creep rate, and $\dot{\varepsilon}_d = \dot{\varepsilon}_r$. However, the mean recrystallized grain size D might adjust itself to a different relative contribution of dislocation and diffusion creep, defined

$$\dot{\varepsilon}_d/\dot{\varepsilon}_r = C \tag{12}$$

Here, C may depend upon σ and temperature but can be assumed constant for sufficiently small ranges of these variables. Taking now d=D, i.e., assuming a steady state recrystallized grain size, and combining Eqs. (5), (10), (11), and (12) results in:

$$D = K_7 \sigma^{-(n-1)/p} \exp\left(\frac{Q_r - Q_d}{pRT}\right) \tag{13}$$

with $K_7=(A/CB)^{1/p}$, where C takes the value 1 for exact correspondence with the mechanism boundary.

Comparison of above models

The model of the stress-dependence of both subgrain and recrystallized grain size advanced by Twiss (1977) has been criticized in the literature (Poirier 1985; Derby 1990) because it rests on an incorrect application of equilibrium thermodynamics to what is clearly a non-equilibrium, dynamic process as both subgrains and new grains are cyclically formed and removed during syntectonic recrystallization. The stable grain size predicted by Twiss is the smallest grain size possible; the system, however, can always lower its energy by allowing these small grains to grow (Poirier 1985). Although widely applied in the past, the Twiss model must therefore be regarded as a lower bound only (see also Twiss and Sellars 1978), and the model cannot accordingly be generally used. The model of the stress dependence of subgrain size developed by Edward et al. (1982) overcomes the criticism of Twiss' model because it is based on a dynamic balance between arrival and annihilation of dislocations at subboundaries, rather than assuming an equilibrium state. In further contrast to the Twiss subgrain size relation (3), the stress exponent m in the Edward model is dependent on the creep behavior of the respective material, and the d_s–σ relationship includes activation energy terms. Consequently, the d_s–σ relationship is dependent on temperature if Q_{cl} is not equal to Q_r. This would be the case, for example, if dislocation climb in the subgrain wall were controlled by pipe diffusion ($Q_{cl}<Q_v$), while creep were controlled by lattice diffusion (i.e., $Q_r=Q_v$). At high temperature, the steady state subgrain size will then be smaller than at lower temperature at the same stress. Alternatively, dislocation climb in the sub-boundary may be controlled by lattice diffusion ($Q_{cl}=Q_v$), while creep may be controlled by dislocation cross slip ($Q_r<Q_v$). The steady state subgrain size will then increase with increasing temperature.

The recrystallized grain size versus stress relations of Derby and Ashby [Eq. (7)], of Shimizu [Eqs. (8) and (9)], and following from the GSI–GSS field boundary hypothesis [Eq. (13)] have similar forms. Most importantly, all three contain activation energy terms. Given that, in general, $Q_{gb}\approx 0.6Q_v$ (Frost and Ashby 1982; Evans and Kohlstedt 1995), the D–σ relationships for nucleation by both grain boundary bulging (Derby/Ashby) and progressive subgrain rotation (Shimizu) are expected to be (weakly) temperature dependent. At high temperature, the steady state recrystallized grain size will then be smaller than at lower temperature at the same stress. In the case of the field boundary equation [Eq. (13), covering both migration and rotation recrystallization], a temperature dependence is also expected, except when GSS and dislocation (GSI) creep are both controlled by lattice diffusion [i.e., $(Q_r=Q_v)=Q_d$]. At high temperature (at constant stress), the recrystallized grain size D will be smaller than at low temperature if $\Delta Q>0$, i.e., if $Q_r>Q_d$ (cf. Derby/Ashby and Shimizu's relations) whereas the opposite would hold if $\Delta Q<0$, i.e., if $Q_r<Q_d$. The latter would be the case if, for example, diffusion (GSS) creep is controlled by lattice diffusion, while recovery (GSI) creep is controlled by dislocation cross slip. Note that the stress exponent m [cf. Eq. (1)] in the Derby/Ashby and field boundary equations depends on the creep behavior, whereas it is a material independent constant in Shimizu's relations.

The above comparison of model predictions shows that subgrain size versus stress relations as well as recrystallized grain size versus stress relations are in general expected to show a temperature dependence. In addition, the relations may involve a dependence upon the creep behavior of the material, depending on the mechanism or combination of mechanisms of new grain nucleation. To date, neither the temperature dependence nor dependence upon creep behavior have received much attention in the literature. In the next section, we will examine experimentally calibrated D–σ relations from the literature in this framework, i.e., we will try to evaluate which models are supported by experimental data.

Experimental data versus models

In Table 1, a compilation is presented of m-values from experimentally calibrated d_s–σ and D–σ relations obtained for a range of metals, rocks and rock analogues by fitting Eq. (1) to the experimental data (i.e., either fitted at constant temperature or assuming no dependence on temperature). We distinguish between rotation and migration recrystallization only if explicitly differentiated in the respective study. Added to the table are values for the power law stress exponent n [Eq. (5)], as reported in the same study or other literature.

Table 1 Compilation of *m*-values from experimentally calibrated d_s–σ and D–σ relations for a range of materials. Values for the power law stress exponent n [Eq. (5)] as reported in the same study or other literature. *m*-values obtained by fitting Eq. (1) to the experimental data. In some studies, σ–d data were graphed without giving actual values for *m* and/or n. In those cases, we performed the best fit regression analysis; these results are given in italics

Material	m1[a]	m2[b]	m3[c]	m4[d]	n	References
Albitic feldspar				0.66	*3.1*	Post and Tullis (1999)
Al	1.18				4.5	Edward et al. (1982)
Al	1.00				4.4	Takeuchi and Argon (1976); Frost and Ashby (1982)
Al	0.26				4.4	Takeuchi and Argon (1976); Frost and Ashby (1982)
Al	0.70				4.4	Takeuchi and Argon (1976); Frost and Ashby (1982)
Al	0.62				4.4	Twiss (1977); Frost and Ashby (1982)
Calcite (Carrara marble)			*0.89*		7.6	Schmid et al. (1980), regime 2
Calcite (Carrara marble)			*0.97*		4.2	Schmid et al. (1980), regime 3
Calcite (Carrara marble)			1.14	1.12	7.6	Rutter (1995); Schmid et al. (1980)
Calcite gouge		1.42			4.7	Friedman and Higgs (1981); Schmid et al. (1980)
Cu		1.24			4.8	Derby and Ashby (1987); Frost and Ashby (1982)
Cu	1.00				4.8	Takeuchi and Argon (1976); Frost and Ashby (1982)
Cu (0–8% Al)		1.52			4.8	Twiss (1977); Frost and Ashby (1982)
Cu	0.98				4.8	Twiss (1977); Frost and Ashby (1982)
α-Fe		1.59			6.9	Luton and Sellars (1969); Frost and Ashby (1982)
α-Fe (vacuum melted)	0.83	1.41			4.1	Glover and Sellars (1973)
α-Fe	0.40				4.5	Orlova et al. (1972); Pahutova et al. (1973)
Fe – 3%Si	1.39				5.8	Edward et al. (1982)
Fe – 3%Si	1.85				5.8	Twiss (1977); Edward et al. (1982)
Fe – 3%Si	*1.12*				*5.1*	Young and Sherby (1973)
Fe – 25% Cr	*1.19*				*9*	Young and Sherby (1973)
Fe – 4% Mo	0.50				3.2	Takeuchi and Argon (1976); Maruyama et al. (1980)
γ-Fe (low C)	*1.40*				4.5	Sakai (1989); Frost and Ashby (1982)
Halite (Avery island rocksalt)	1.15				4.5	Carter et al. (1993)
Halite (synthetic)	0.84			1.18	4.56	Spiers et al. (in preparation)
Halite single crystals	1.00		1.18	1.28	*4.4*	Guillopé and Poirier (1979)
Ice		*0.85*			*3.5*	Jacka and Li Jun (1994)
Ice		1.37			3.0	Derby and Ashby (1987); Frost and Ashby (1982)
KBr	0.80				4.3	Wolfenstine and Shih (1994)
KI	1.08				4.6	Wolfenstine and Shih (1994)
LiF single crystals <100>	0.83				3.4	Cropper and Pask (1973)
LiF single crystals <111>	1.08				4.1	Cropper and Pask (1973)
LiF single crystals <100>	0.66				4	Streb and Reppich (1973)
Magnox (Mg alloy)		1.28			4.5	Drury et al. (1985)
Magnox (Mg alloy)		1.23			4.3	De Bresser et al. (1998)
MgO single crystals	1.00				3.3	Takeuchi and Argon (1976); Frost and Ashby (1982)
$NaNO_3$	1.18		1.54	1.54	4.4	Tungatt and Humphreys (1984)
Ni		1.33			5.7	Luton and Sellars (1969)
Ni		2.00			5.6	Sah et al. (1974)
Ni	1.08				4.6	Twiss (1977); Frost and Ashby (1982)
Olivine (Åheim dunite, wet)	0.59			*1.19*	4.48	Van der Wal (1993); Van der Wal et al. (1993); Chopra and Paterson (1984)
Olivine (Anita Bay dunite, wet)	0.42			*0.88*	3.35	Van der Wal (1993); Van der Wal et al. (1993); Chopra and Paterson (1984)
Olivine (San Quintin Baja, dry)	1.00	1.23			3.0	Mercier et al. (1977); Kirby and Raleigh (1973)
Olivine (Mt. Burnet dunite, wet)		*0.89*			3.0	Post (1977)
Olivine (Mt. Burnet dunite, wet)	0.69	0.82			3.0	Ross et al. (1980); Post (1977)
Olivine (Mt. Burnet dunite, dry)		*0.75*			*3.6*	Post (1977)
Olivine (Mt. Burnet dunite, dry)	0.62	1.27			3.8	Ross et al. (1980)
Olivine single crystals	0.67	1.18			3.6	Karato et al. (1980); Durham and Goetze (1977)
Pyrite		1.10			7	Cox et al. (1981)
Pyroxene (diopside, dry)		0.90			4.3	Ave Lallement (1978)
Pyroxene (enstatite, wet)		0.85			3	Ross and Nielson (1978)
Quartzite (novaculite)				0.61	2.6	Bishop in: Post and Tullis (1999); Kronenberg and Tullis (1984)
Quartzite (wet Canyon Creek)		1.40			2.6	Mercier et al. (1977); Parrish et al. (1976)
Quartzite (flint, novac.)		0.59			2.65	Koch (1983); Hacker et al. (1990); Christie et al. (1980)
Steel stainless 316, 775 °C	*2.13*				7.9	Young and Sherby (1973); Frost and Ashby (1982)
Steel stainless 316, 900 °C	*1.89*				7.9	Young and Sherby (1973); Frost and Ashby (1982)
Steel stainless AISI 36	3.13				9	Edward et al. (1982)
Steel stainless AISI 36	1.69				6	Edward et al. (1982)
Steel stainless, austenitic	*0.80*				4.5	Fritzemeier et al. (1980)
Steel stainless, austenitic	0.75				4.5	Twiss (1977); Fritzemeier et al. (1980)
Steel (mild, Al killed)		1.70			6.3	Cepeda et al. (1989)

[a] Subgrains
[b] Unspecified recrystallization mechanism
[c] Rotation recrystallization
[d] Migration recrystallization

Temperature dependence

Evidence for a temperature dependence of the (sub)grain size versus stress relation has so far been reported for only a few materials. Streb and Reppich (1973) measured subgrain sizes in single crystals of LiF, and found the expected inverse dependence upon applied stress (m=0.66) and a direct dependence upon temperature (Fig. 2a). Thus at constant stress, the subgrain size was observed to be larger if the deformation temperature was higher. The same effect of temperature has been reported for α–Fe (Orlova et al. 1972). In contrast, data for stainless steel 316 (Young and Sherby 1973) suggest that at constant stress and increasing temperature, the subgrain size decreases (Fig. 2b).

Mercier et al. (1977) mention that recrystallized grain size versus stress data for wet quartzite and dunite appear to show a weak negative temperature dependence of grain size (i.e., the recrystallized grain size becomes smaller at higher temperature), although the relevant data points are not shown. Ross et al. (1980) report a weak positive temperature dependence for wet dunite, with larger recrystallized grain sizes developing at higher deformation temperature. A positive effect of temperature on D can also be deduced from the results of Tungatt and Humphreys (1984) for polycrystalline sodium nitrate. These authors demonstrate that both the d_s–σ and D–σ relation depend on strain rate; if compared at the same stress level this implies variations in (sub)grain size related to temperature. Finally, our work on a magnesium alloy, Magnox Al80, showed a decrease in recrystallized grain size with increasing temperature (Fig. 3) and good agreement with the field boundary hypothesis (De Bresser et al. 1998).

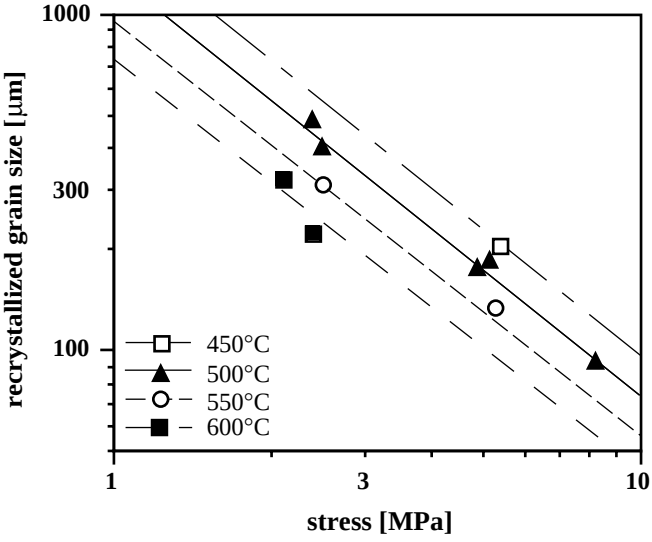

Fig. 3 Recrystallized grain size versus flow stress plotted for the magnesium alloy Magnox Al80, from data of De Bresser et al. (1998). At constant stress, the mean recrystallized grain size decreases with increasing temperature [cf. Eq. (13)]

From the above, it follows that although evidence exists for a modest temperature dependence of (sub)grain size versus stress relations in a few materials, widespread support is lacking. This might reflect (1) that the influence of temperature in fact is very limited, implying small differences (ΔQ) in the activation energies appearing in the model equations; (2) that the scatter in the experimental results for individual materials is usually too large to recognize any effect; or (3) that the experimental program did not

Fig. 2 a,b Subgrain size data plotted versus flow stress for **a** LiF and **b** stainless steel 316, from data of Streb and Reppich (1973) and Young and Sherby (1973), respectively. Values of m (Table 1) as indicated. Note that for both materials, the σ–d_s relationship appears to be temperature dependent [cf. Eq. (6)], although with opposite sense regarding the change in subgrain size with increasing temperature

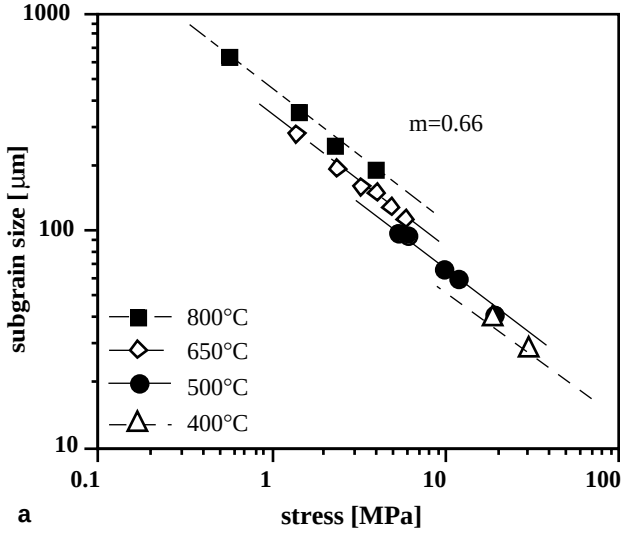

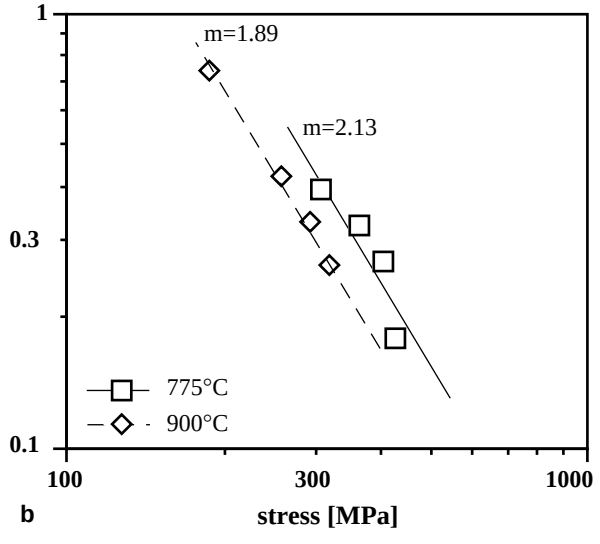

systematically explore the possible role of temperature. With respect to point (3), we note that, to investigate a wide enough stress range at laboratory accessible strain rates, the majority of previously obtained D–σ relations were calibrated by combining low temperature/high stress data with high temperature/low stress data, assuming no influence of temperature and therefore obscuring any such effect.

Stress dependence of D–σ relations

Values for the exponents m and n in Table 1 are plotted against each other in Figs. 4 and 5, for subgrains and recrystallized grains, respectively. Included in the figures are the trends as predicted by the various models considered above.

The results relating to subgrain size versus stress data (Fig. 4) show considerable scatter, with m ranging from 0.4 to 3.1. A substantial proportion of the m-values clearly deviates from the m=1 value implied by the Twiss model [Eq. (3)]. Rather, a trend is apparent that is more in agreement with the model of Edward et al. [1982; Eq. (6)].

The results pertaining to the recrystallized grain size versus stress relations (Fig. 5) also show considerable spread, with m varying between 0.6 and 2. Though the scatter is substantial, some inferences can be made. The data show little support for the Derby and Ashby model [Eq. (7)]; at almost any given n-value, the measured m-exponent is smaller than predicted. Only the data for ice (quoted in Derby and Ashby 1987), wet Canyon creek quartzite and San Quentin Baja dunite (both in Mercier et al. 1977) fall close to the Derby/Ashby prediction. Turning to the Shimizu model, this falls midway in the range of observed m-values, but does not reproduce the tendency for m to increase with n apparent in the data (Fig. 5). As explained already, it is probably not realistic to distinguish in practice between grains explicitly resulting from rotation or migration recrystallization. Nonetheless, a few values for m are quoted to represent "rotation" recrystallization in Table 1; these mostly lie below the values predicted by Shimizu's model [Eqs. (8) and (9)]. Like the Shimizu model, the Twiss predictions (m=1.3–1.5) fall midway in the range of observed values (Fig. 5). However, in the light of the flaws in this model, an agreement appears to be fortuitous, and again the tendency of m to increase with n is not reproduced. Let us lastly compare the data with the predictions of our field boundary hypothesis. This demonstrates that the majority of the data points falls close to the range defined by the field boundary hypothesis Eq. (13), assuming p-values in

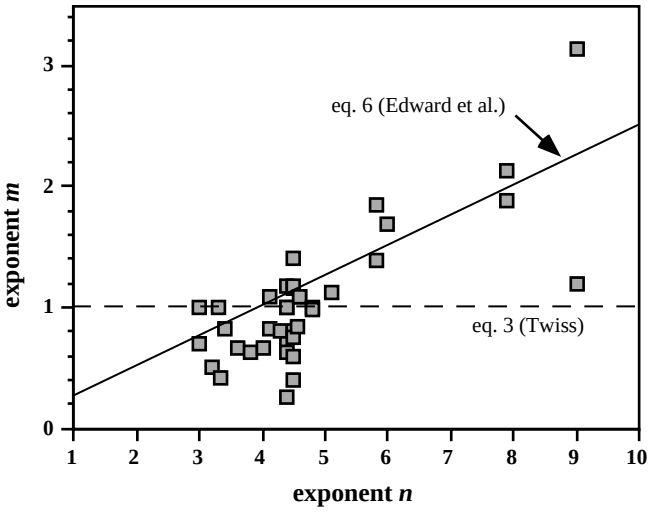

Fig. 4 Values of m in the subgrain size versus stress relations, obtained for a wide range of materials, plotted versus the (Dorn) power law stress exponent n [GSI creep law, Eq. (5)] after Table 1. Added to the plot are the trends predicted by Eqs. (3) (Twiss model for subgrain size versus stress) and (6) (Edward model)

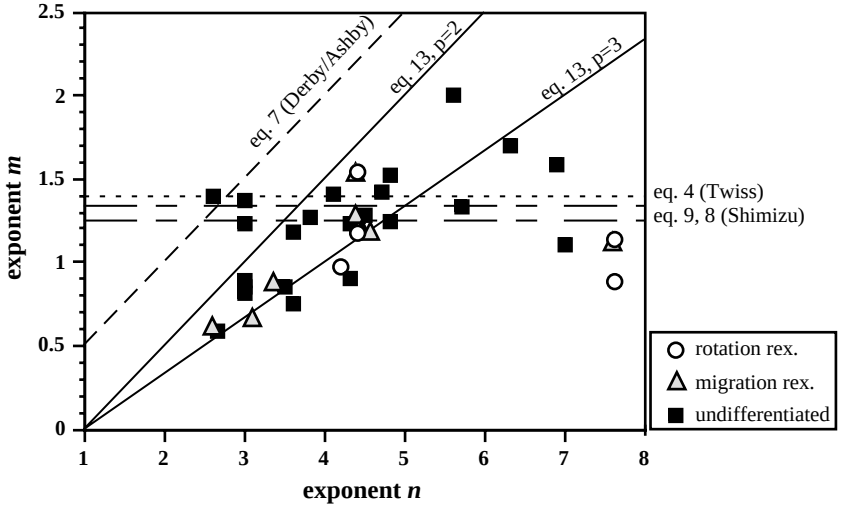

Fig. 5 Values for m in the recrystallized grain size versus stress relations plotted against the (Dorn) power law stress exponent n for a wide range of materials, after Table 1. Added to the plot are the trends predicted by Eqs. (4) (Twiss model for recrystallized grain size versus stress), (7) (Derby/Ashby model), (8) and (9) (Shimizu model), and (13) (field boundary hypothesis with p=2 for lattice diffusion, and p=3 for grain boundary diffusion)

the range between p=2 and p=3. Note from Table 1 that not enough systematic m versus n data are available to resolve with confidence any trends pertaining to individual materials.

Field boundary hypothesis tested for olivine and calcite

We now evaluate in detail the applicability of the field boundary hypothesis to dynamic recrystallization in two important Earth materials, namely olivine and calcite. First, we compile all available D–σ data. Then data for a given temperature are plotted in a series of deformation mechanism maps. The maps are drawn using experimentally determined flow laws to outline the GSS and GSI deformation fields in grain size versus stress space (Frost and Ashby 1982; Fig. 1). Ideally, one would prefer to use D–σ data derived from the same set of experimentally deformed samples as used to derive the GSI and GSS flow laws. In practice, we know of no study in which the same set of experiments has been used to explore both the dislocation creep and the diffusion creep behavior, and for which the D–σ relationship has also been calibrated. Thus, we have to rely on the merging of data and flow laws from different starting materials and/or experiments. An additional problem is the question of whether or not microstructural and mechanical steady state was reached in the various experiments merged. Note that natural strains larger than 0.6 were required to obtain stable grain sizes in Magnox (Drury et al. 1985). In constructing the deformation mechanism maps, composite flow laws embodying GSI and GSS creep were used (e.g., Freeman and Ferguson 1986), resulting in gently curved strain rate contours rather than the abrupt changes shown in Fig. 1, which assumes a sharp transition. The individual flow laws used for the maps drawn are tabulated in Table 2.

Olivine

Recrystallized grain size-stress data for olivine have been obtained from high temperature (mainly T=1500 °C) creep tests on San Carlos single crystals (Karato et al. 1980), and somewhat lower temperature experiments on polycrystalline samples of Mt. Burnet dunite (Post 1977; Ross et al. 1980; 900–1400 °C), Åheim dunite and Anita Bay dunite (Van der Wal et al. 1993; 1100–1300 °C). These D–σ data are shown in Fig. 6a. Although a general trend in recrystallized grain size as a function of flow stress is apparent, the data show considerable scatter. In particular, the data obtained for Mt. Burnet dunite show a wide spread compared with the results for the Åheim and Anita Bay dunite. This mainly reflects the use of a solid medium deformation apparatus in the case of the Mt. Burnet material, whereas the latter dunites were deformed in a (Paterson) gas apparatus, in which stress measurement is generally considered more accurate. The large scatter in the entire set of data precludes any reliable conclusion regarding the possible influence of temperature on recrystallized grain size (Fig. 6b). The individual data sets for Åheim and Anita Bay dunite (Van der Wal et al. 1993) are better constrained in terms of flow stress level, but are not extensive enough to systematically explore the role of temperature. However, because of their relative accuracy, the Åheim/Anita Bay data are preferred for the purpose of comparison with deformation mechanism maps.

Four alternative deformation mechanism maps have been constructed by combining dislocation creep equations for Åheim dunite and Anita Bay dunite (Chopra and Paterson 1981, 1984) with the GSS creep equations for synthetic olivine aggregates given by Karato et al. (1986 – hot pressed, crushed San Carlos single crystals) and from McDonnell (1997; McDonnell et al. 1999 – pure Mg-forsterite fabricated using a sol-gel based technique). All maps represent wet olivine behavior at 1250 °C. In the map of Fig. 7d (Anita Bay dunite + sol-gel based forsterite) the D–σ data

Table 2 Overview of experimentally derived flow laws for olivine and calcite employed in the construction of the deformation mechanism maps of Figs. 7 and 9

Material	A, B ($MPa^{-n}\ \mu m^{-p}\ s^{-1}$)	Q (kJ/mol)	p	n	Reference
Olivine (Fig. 7)					
1. Åheim dunite (wet), GSI	4.17E+02	498	-	4.5	Chopra and Paterson (1981, 1984)
2. Anita Bay dunite (wet), GSI	9.55E+03	444	-	3.4	Chopra and Paterson (1981, 1984)
3. Synth. San Carlos (wet), GSS	1.50E+06	250	3	1	Karato et al. (1986)
4. Synth. Forsterite (wet), GSS	4.74E+04	302	3	2.1	McDonnell (1997)
Calcite (Fig. 9)					
5. Carrara marble, GSI	1.26E+03	420	-	7.6	Schmid et al. (1980), regime 2
6. Carrara marble, GSI	1.26E+08	428	-	4.2	Schmid et al. (1980), regime 3
7. Synthetic calcite, GSS[a]	1.00E+02	190	1.34	3.3	Walker et al. (1990), intermediate σ/T
8. Synthetic calcite, GSS	8.51E+04	190	1.87	1.7	Walker et al. (1990), low σ/high T

[a] Equation (7) was not used in map construction because it probably represents composite GSI/GSS behavior (see text)

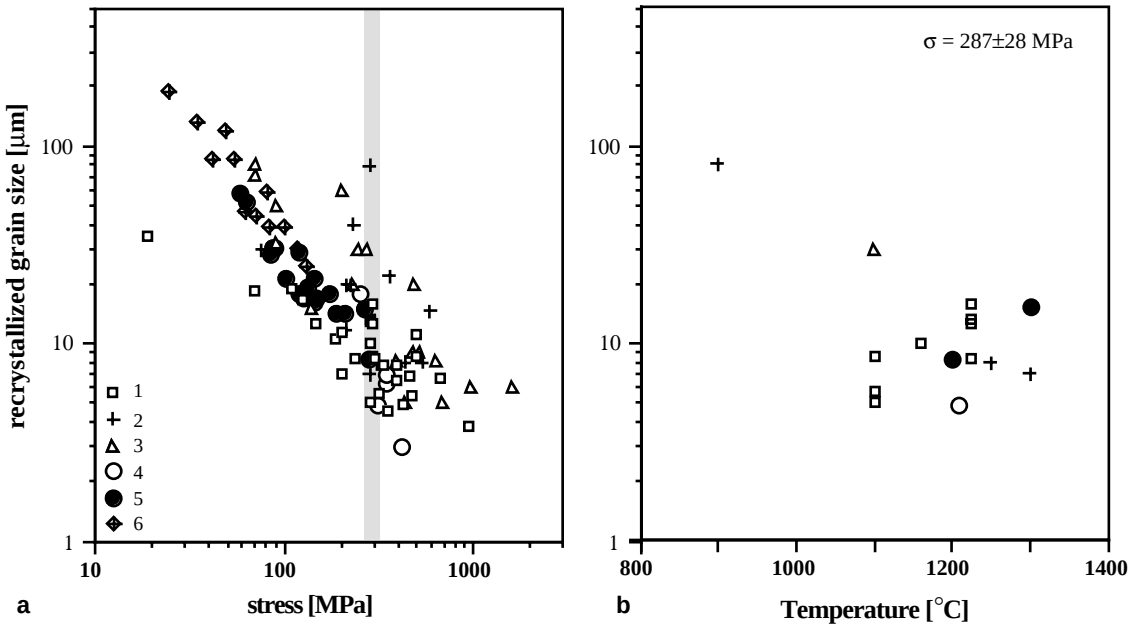

Fig. 6 a,b Compilation of recrystallized grain size versus flow stress data for olivine. **a** *1* Data of Ross et al. (1980 – Mt Burnet dunite); *2*, *3* Post (1977 – Mt. Burnet dunite, dry and wet, respectively); *4*, *5* Van der Wal et al. (1993 – Åheim/Anita Bay dunite, dry and wet, respectively); *6* Karato et al. (1980 – San Carlos single crystals). *Dotted band* indicates the flow stress range for which **b** is constructed. **b** Recrystallized grain sizes obtained at a flow stress of 287±28 MPa, plotted as a function of temperature. See text for discussion

plot well into the GSI field. However, all other three maps show a close correspondence between the plotted D–σ data (gas apparatus) and the GSS–GSI transition region.

Calcite

Recrystallized grain size versus stress data for calcite (Fig. 8a) have been obtained by Schmid et al. (1980) and Rutter (1995) for Carrara marble, and by Friedman and Higgs (1981) for calcite fault gouge. For Carrara marble, a subdivision was made by both Schmid et al. and Rutter between grains recrystallized by rotation and by migration mechanisms. As a criterion for the distinction, the size of the grains was used: equiaxed new grains on the scale of subgrains were assumed to have developed by rotation mechanisms, whereas large grains were assumed to develop by migration recrystallization. The D–σ data show clear trends (Fig. 8a) but considerable scatter, as in the case of olivine (cf. Fig. 6a). This again precludes conclusions regarding any influence of temperature on recrystallized grain size (Fig. 8b).

For the construction of the deformation mechanism maps (Fig. 9), we used the GSI dislocation creep laws obtained for Carrara marble by Schmid et al. (1980) and the GSS flow law for synthetic calcite aggregates obtained by Walker et al. (1990). A subdivision into two power law GSI creep regimes was made by Schmid et al. (1980; see Table 2) to account for the experimentally observed decrease in n-value with decreasing stress and increasing temperature. In fact, this subdivision is somewhat artificial because later work on Carrara marble has demonstrated a gradual change in n with stress and temperature rather than an abrupt change (Chopra et al. 1988; De Bresser 1996). Thus, to explore the variability in possible deformation mechanism maps, we applied both the regime 2 and regime 3 flow laws of Schmid et al. (1980). Also, the GSS creep field of Walker et al. (1990) was subdivided by these authors in two regimes (Table 2). However, we chose not to use their higher stress GSS regime because the relatively high value of n=3.3 suggests that this flow law represents some combination of GSI and GSS creep, already accounted for in our deformation mechanism maps. Note that the D–σ data are consistently positioned within the GSS–GSI transition region in the map of Fig. 9b. In the map of Fig. 9a, however, less than half of the data points fall in the transition region.

Discussion

The Derby/Ashby and Shimizu models addressing the relationship between dynamically recrystallized grain size and flow stress, discussed in this paper, comprise end-member models for rotation and migration recrystallization. In our own approach (field boundary hypothesis), both recrystallization mechanisms may be involved whereas grain size is determined in relation to the mechanical behavior. The literature data com-

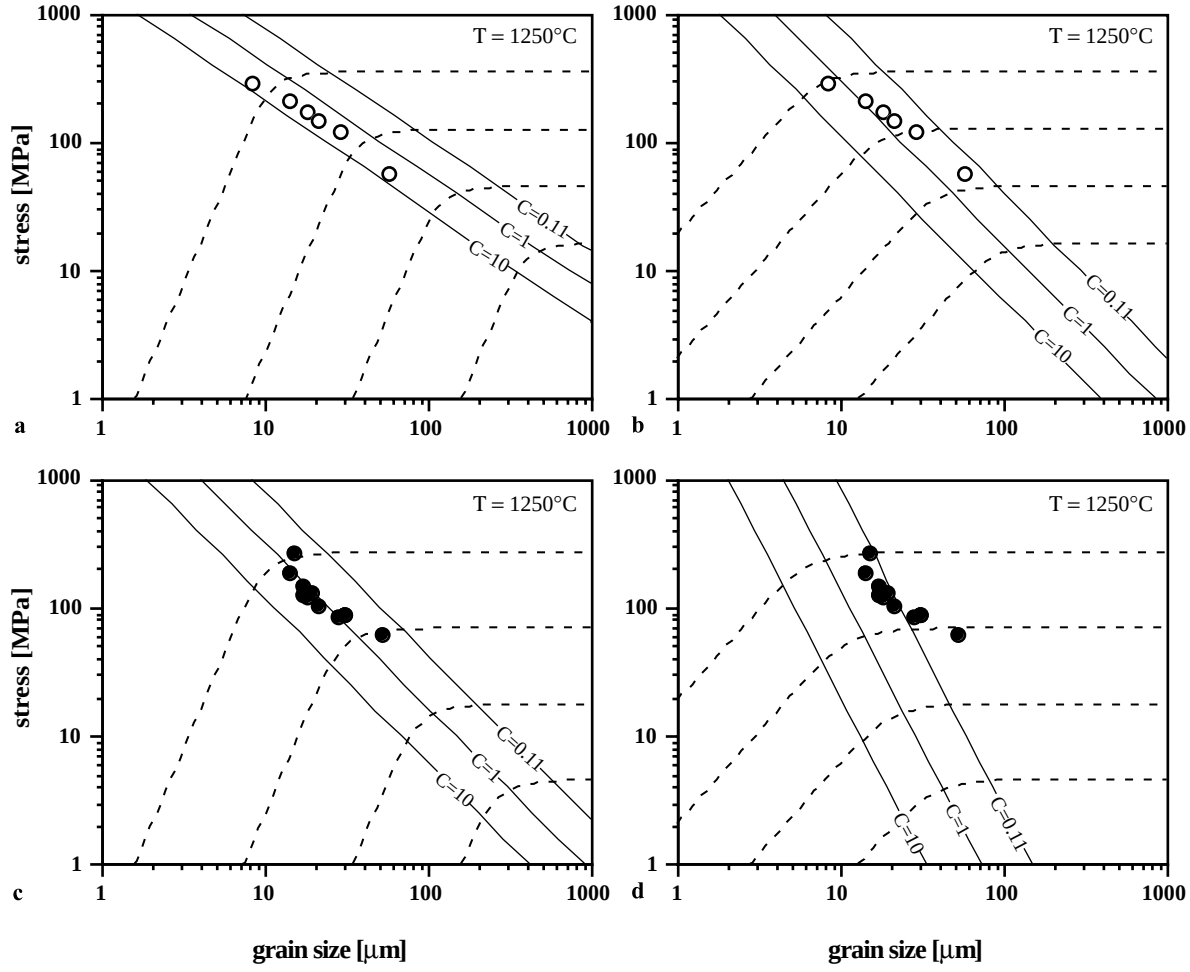

Fig. 7a–d Deformation mechanism maps for wet olivine at T=1250 °C, plotted using the constitutive creep equations tabulated in Table 2. **a** Flow laws 1 (Åheim dunite GSI) and 3 (synthetic San Carlos GSS); **b** flow laws 1 (Åheim dunite GSI) and 4 (synthetic forsterite GSS); **c** flow laws 2 (Anita Bay dunite GSI) and 3 (synthetic San Carlos GSS); **d** flow laws 2 (Anita Bay GSI) and 4 (synthetic forsterite GSS). *Dashed lines* are contours for strain rates of 10^{-3}, 10^{-5}, 10^{-7} and 10^{-9} s^{-1}. *Straight lines* for C=0.11, C=1 and C=10 indicate the relative contributions of GSS and GSI creep to the overall creep rate in the mechanisms transition region, see Eqs. (11) and (12). The *open* and *closed circles* represent D–σ data points (T=1200–1300 °C) for Åheim and Anita Bay dunite, respectively, taken from Van der Wal et al. (1993)

piled in Fig. 5 lend support to the boundary hypothesis rather than to the end-member models because the data better fit the range defined by the GSI–GSS boundary equation [Eq. (13), for $2 \leq p \leq 3$] than the model predictions for either migration recrystallization [Derby and Ashby; Eq. (7)] or rotation recrystallization [Shimizu; Eqs. (8) and (9)]. However, uncertainties and scatter in the available (literature) data preclude definitive statements. Nevertheless, support for the boundary hypothesis also comes from the correspondence of independently obtained D–σ data with the GSS–GSI transition region as demonstrated in the deformation mechanism maps plotted for olivine and calcite (Figs. 7 and 9). Finally, it is recalled that our earlier results on the magnesium alloy Magnox Al80 (De Bresser et al. 1998) are also in good agreement with the hypothesis embedded in Eq. (13).

We will now discuss the consequences of our model should it apply generally. These relate to (1) the impact on grain size paleopiezometry, (2) the expected rheological weakening caused by dynamic recrystallization, and (3) the interpretation of the stress–strain behavior measured in laboratory deformation experiments.

Paleopiezometry

Experimentally calibrated D–σ relationships have frequently been used for estimating paleo-stresses in naturally deformed rocks (e.g., Kohlstedt and Weathers 1980; Pfiffner 1982; Ord and Christie 1984; Hacker et al. 1992; Fliervoet 1995). Invariably, the applied D–σ relations did not include temperature as an environmental variable. In view of the above discussion on (1) the role of temperature in the various recrystalliza-

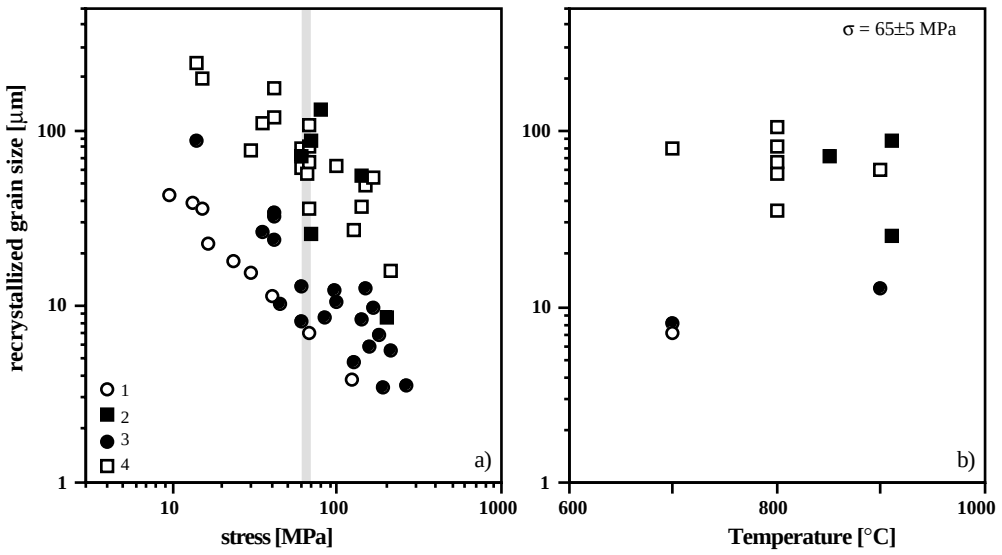

Fig. 8 a,b Compilation of recrystallized grain size versus flow stress data for calcite. **a** *1* Data of Schmid et al. (1980 – Carrara marble, rotation recrystallization); *2* Friedman and Higgs (1981, fault gouge); *3*, *4* Rutter (1995 – Carrara marble, rotation and migration recrystallization). *Dotted band* indicates flow stress range from which **b** is constructed. **b** Recrystallized grain sizes obtained at a flow stress 65±5 MPa, plotted as a function of temperature. See text for discussion

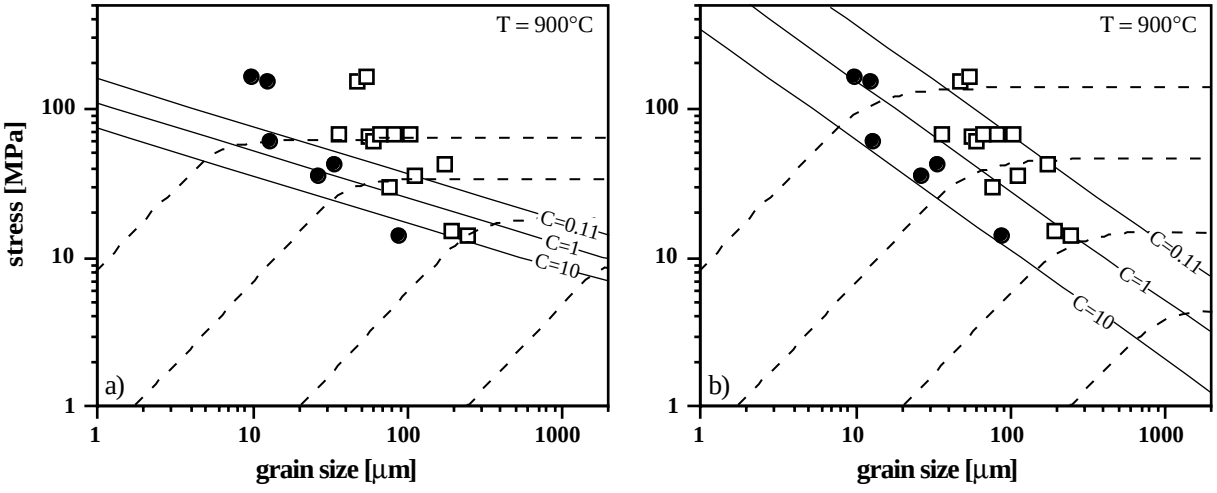

Fig. 9 a,b Deformation mechanism maps for calcite at T=900 °C, drawn using the constitutive creep equations tabulated in Table 2. **a** Flow laws 5 (Carrara marble GSI regime 2) and 8 (synthetic calcite GSS); **b** flow laws 6 (Carrara marble GSI regime 3) and 8 (synthetic calcite GSS). *Dashed lines* are contours for strain rates of 10^{-2}, 10^{-4}, 10^{-6} and 10^{-8} s^{-1}. *Straight lines* drawn for C=0.11, C=1 and C=10 indicate the relative contributions of GSS and GSI creep to the overall creep rate in the mechanism transition region, see Eqs. (11) and (12). The *closed circles* and *open squares*, respectively represent D–σ data points (T=800–1000 °C) obtained for rotation and migration recrystallization in Carrara marble by Rutter (1995)

tion models, and (2) the available, though limited, experimental evidence for the influence of temperature, this may have been erroneous. Because natural deformation usually occurs at lower temperatures than applied during experimental calibration of most piezometric relations, paleo-stresses calculated from existing piezometers may represent over- or underestimates depending on the relative values of the activation energy terms appearing in the relevant model equations. For the field boundary Eq. (13), the temperature dependence drops out if GSS creep and dislocation creep are rate controlled by the same mechanism, e.g., by lattice diffusion. However, if grain boundary diffusion controls GSS creep, then $Q_{gb} \approx 0.6 Q_r$ (Frost and Ashby 1982; Evans and Kohlstedt 1995), and paleo-stresses estimated without taking temperature into account will be underestimated compared with the true values. The error could be as high as an order of magnitude, as demonstrated in Fig. 10 for olivine and calcite. We emphasize that an accurate, revised calibration of D–σ relations, involving a systematic investigation of the role of temperature and reaching true steady state, is required before any firm significance can be attributed to the results depicted in Fig. 10. Nevertheless, temperature might be of more importance in grain size paleo-piezometry than hitherto assumed, and the proposed revision of D–σ relations seems essential if they are to be applied with any confidence for materials such as calcite and olivine.

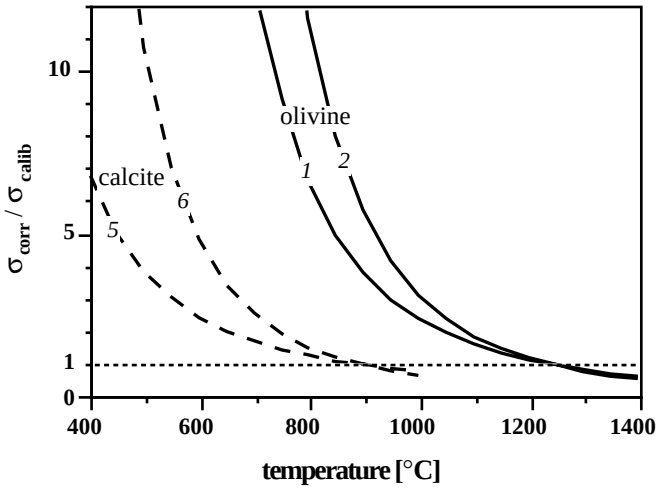

Fig. 10 Illustration of the potential error in flow stress estimation obtained if a grain size piezometer is used that does not take temperature into account. Recrystallization is taken to be controlled by the field boundary Eq. (13) with $Q_{gb} \approx 0.6 Q_r$ (i.e., when GSS creep is controlled by grain boundary diffusion). The ratio $\sigma_{corr}/\sigma_{calib}$ represents the multiplication factor required to correct the stress at the temperature of experimental calibration (σ_{calib}) to the actual, corrected stress at the temperature of interest (σ_{corr}). *1, 2* Olivine using GSI flow laws 1 and 2, respectively (Table 2); *5*, *6* calcite, using flow laws 5 and 6 from Table 2. The ratio $\sigma_{corr}/\sigma_{calib}$ is higher than 1 for all temperatures lower than the calibration temperature (1250 °C for olivine, 900 °C for calcite). The corrected value therefore is always larger than σ_{calib}. Failing to take temperature into account thus might result in underestimates of flow stress up to an order of magnitude

Rheological weakening

The field boundary model implies that through recrystallization, deformation becomes controlled by combined GSS and dislocation mechanisms, and the grain size organizes itself in the GSS–GSI boundary. The resulting steady state strain rate during dynamic recrystallization is the sum of the contributions of dislocation and diffusion creep, and can be expressed using Eqs. (11), (12) and (5) as

$$\dot{\varepsilon}_{rx} = \dot{\varepsilon}_d + \dot{\varepsilon}_r = (C+1)\dot{\varepsilon}_r = (C+1)B\sigma^n \exp\left(\frac{-Q_r}{RT}\right) \quad (14)$$

The steady state creep during dynamic recrystallization thus can be expressed using a grain size insensitive constitutive rate equation [Eq. (14)]. Compared with dislocation creep before pervasive recrystallization [Eq. (5)], only minor weakening is therefore possible as a result of grain size reduction by dynamic recrystallization. This is seen from Eq. (14) which shows that, at constant stress, the strain rate is enhanced by a factor of only (C+1). If both dislocation and diffusion creep contribute equally to the total strain rate, C=1 [see Eq. (12)] and the strain rate at the boundary will be just twice as fast as before recrystallization. Conversely, Eqs. (5) and (14) can also be compared for a fixed steady state strain rate, in order to express the rheological weakening in terms of a change in steady state flow stress level, from σ_r before or without recrystallization dislocation creep, Eq. (5) to σ_{rx} during recrystallization. This yields

$$\sigma_{rx} = \sigma_r (C+1)^{-1/n} \quad (15)$$

Note that σ_{rx} accordingly falls in the GSI–GSS boundary [Eq. (14)]. Calculated ratios of σ_{rx}/σ_r are plotted for various values of C and n in Fig. 11. This suggests that for a value of n ≈3 typical for dislocation creep, the stress decrease caused by dynamic recrystallization as described by the field boundary model is ~20% if both GSI and GSS mechanisms contribute equally to the overall creep rate (C=1). This increases to ~50% if the overall creep rate is strongly dominated by GSS creep (C≈10). For $n \approx 8$ (e.g., calcite, see Table 2), the stress decreases <10% for C=1.

The above implies that, at constant temperature, grain size reduction by dynamic recrystallization is not expected to result in a major change in strength or effective viscosity of a material deforming in steady state. These findings will influence numerical modeling performed to determine the conditions under which strain localization takes place (e.g., Kameyama et al. 1997; Braun et al. 1999). These conditions play an important role in large-scale models of lithosphere deformation and mantle flow.

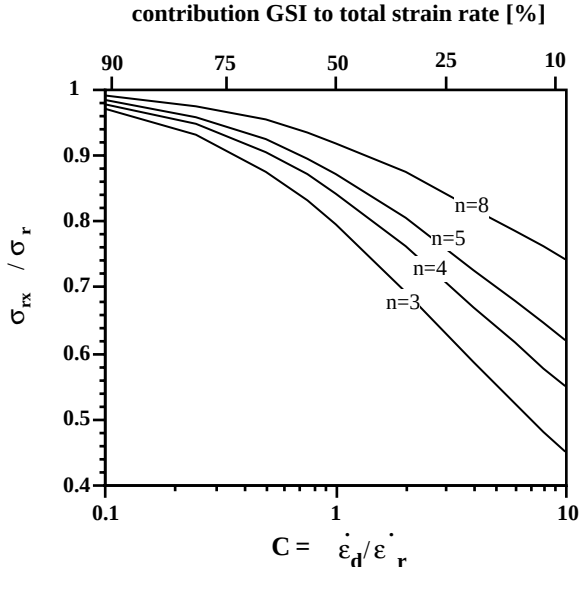

Fig. 11 Rheological weakening as a consequence of dynamic recrystallization leading to a balance between grain size reduction and grain growth at the GSI–GSS boundary. σ_r represents the flow stress for steady state GSI (dislocation) creep at low strain, before pervasive recrystallization. σ_{rx} indicates the reduced flow stress governed by the field boundary model expressed in Eq. (14). Ratios σ_{rx}/σ_r were calculated using Eq. (15), for the values of C and n shown

Interpretation of constant strain rate experiments

On the basis of experiments and the models discussed here, single step deformation experiments achieving high strain at constant strain rate and high temperature are expected to result in an evolution in microstructure demonstrating either grain size reduction by dynamic recrystallization or grain growth if the starting grain size is small and/or the strain rate is low. Associated with this evolution, a decrease or increase in flow stress might be expected, as shown in Fig. 12a for 60/40 brass. In the framework of the field boundary model, we expect progressive evolution towards a balance between grain size reduction and grain growth, at a reduced stress compared with the flow stress required for dislocation creep without recrystallization (at the same strain rate and temperature). High temperature stress–strain curves with a clear peak followed by weakening (see Fig. 12b) might accordingly be interpreted as demonstrating the onset of steady state dislocation (GSI) creep at the peak stress, followed by dynamic recrystallization and strain softening until a balance has been achieved between grain size reduction and grain growth at conditions corresponding to the GSI–GSS boundary. Preliminary results of high strain torsion experiments on anhydrite (Stretton and Olgaard 1997) and Carrara marble (Pieri et al. 1998) at high temperature appear to be explained in this way. In particular the work on Carrara marble has shown peak stresses followed by a weakening of 5–7% reaching steady state flow with n≈8–9. This behavior agrees well with the predictions of Fig. 11. Results obtained from stepping experiments on anhydrite suggest that dynamic recrystallization causes a clear-cut switch from GSI to GSS creep. However, step strains may have been too small to achieve true steady state behavior in accordance with the field boundary model.

It is important to note at this point that processes other than dynamic recrystallization can result in material weakening (see Poirier 1980; Rutter 1999), such as geometrical softening caused by development of a crystallographic preferred orientation of original or recrystallized grains, or thermal softening because of shear heating. A systematic experimental investigation of recrystallization should thus include deformation tests on fine grained starting material in order to test for the progressive evolution suggested in Fig. 12.

Final remarks

We now consider a number of outstanding points not adequately discussed in the foregoing.

First, in compiling the stress exponents m in Table 1, almost all values presented in the various studies cited have been taken at face value. As a consequence, recrystallized grain size versus stress relations using different grain size measurement and averaging techniques have been treated on equal footing. Although linear intercept methods have been used in most studies, the increasing availability of image analysis techniques has promoted the use of equivalent circular diameters (ECD; e.g., Heilbronner and Bruhn 1998) derived from grain areas in more recent studies. Moreover, some studies incorporated stereological corrections for sectioning effects, although the applied correction factor is not always consistent from one study to the next. Finally, although the grain size is usually expressed as an arithmetic mean, it has been found in recent years that the recrystallized grain size often shows a log-normal distribution, hence the geometric mean (median) gives a better representation of the grain microstructure (e.g., Ranalli 1984; Newman

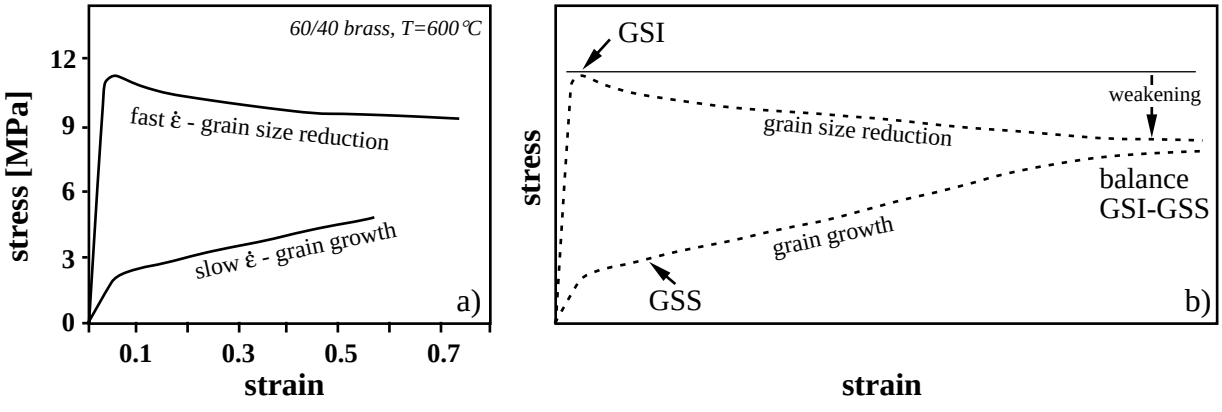

Fig. 12 **a** Stress–strain curves for 60/40 brass at T=600 °C from McQueen and Baudelet (1980), showing weakening during grain size reduction at fast strain rate, and hardening caused by grain coarsening at slow strain rate. **b** Possible interpretation of the stress–strain curves of **a**, in terms of the field boundary hypothesis. At high stress and high strain rate, deformation starts from a single GSI (dislocation) creep mechanism, and evolves towards simultaneous control by GSI and GSS mechanisms, producing minor weakening after a peak stress. Conversely, at sufficiently low stress and strain rate, the material initially deforms by GSS mechanisms, until grain growth results in an increased contribution of dislocation GSI processes and eventually in dual mechanism control once again

1994). We expect that the scatter in the data apparent in Figs. 4 and 5, for example, can be reduced significantly if a consistent approach to grain size measurement and averaging is followed in future.

Next, recall that the cross-cutting by a D–σ relation of the GSI–GSS boundary seen in deformation mechanism maps (Fig. 1), formed the basis for the original notion that dynamic recrystallization can result in a switch in deformation mechanism from GSI to GSS creep with associated major rheological weakening. However, the construction of a deformation mechanism map and the location of mechanism boundaries are subject to considerable uncertainty because of the variability of available flow laws for the relevant mineral (e.g., Figs. 7 and 9), and the degree of freedom in combining different materials (e.g., natural dunite with synthetic polycrystalline olivine or pure forsterite, Fig. 7). Combined with the substantial scatter in measured rheological D–σ data (Figs. 6 and 8), experimental evidence for the occurrence of a mechanism switch during progressive recrystallization thus appears flimsy. Arguments to this have been put forward previously by Etheridge and Wilkie (1979), Zeuch (1983) and Jaroslow et al. (1996). We emphasize this because our field boundary model directly relates dynamic recrystallization to rheology and implies that a switch in deformation mechanism and associated major weakening cannot occur. Nevertheless, highly localized deformation zones with strongly reduced grain sizes do occur in nature. Major weakening in such zones would therefore seem possible only if grain size refinement is caused by a process other than dynamic recrystallization (such as cataclasis or metamorphic reaction), or if grain growth is inhibited. In the case of inhibited grain growth, we propose that the recrystallized grain size versus stress relation will approach the subgrain size versus stress relation in the limiting case.

Third, the field boundary hypothesis represented by Eq. (13) as yet lacks a detailed microphysical basis. We are currently working on formulating such a model in terms of realistic microphysical processes including rotation and migration recrystallization as well as the mechanisms controlling creep rate (GSI and GSS mechanisms). The poor fit of the widely used $d_s \propto \sigma^{-1}$ [Eq. (3)] relation to subgrain size versus stress data (Fig. 4) suggests that the relation should not be included in this form in models for dynamic recrystallization.

Lastly, dynamic recrystallization of materials will in general involve some combination of the basic rotation and migration processes (Drury et al. 1985; Drury and Urai 1990). In practice, it will be difficult to classify microstructures, or individual new grains, in terms of one specific end-member recrystallization mechanism. For that reason, we feel that quantification of dynamically recrystallized grain size should focus on the characterization of grain size distributions rather than on attempts to obtain single values representing migration or rotation recrystallization.

Summary and conclusions

1. Just two microphysical models exist that realistically underpin the empirically well-established relation between recrystallized grain size D and flow stress σ given $D \propto \sigma^{-m}$. These models (because of Derby and Ashby 1987; Shimizu 1998) contain activation energy terms and consequently show a temperature dependence. The value for m is either constant or dependent on the creep behavior of the recrystallizing material via the Dorn power law exponent n. The widely quoted model for the (sub)grain size versus stress relation by Twiss (1977) does not predict a temperature effect, but lacks general applicability.
2. During large-strain deformation, progressive grain size reduction accompanying dislocation creep might be balanced by grain growth at the boundary between grain size insensitive (GSI) dislocation creep and grain size sensitive (GSS) diffusion creep. The D–σ relationship at steady state will then correspond to the equation delineating the creep field boundary, and in general will be temperature dependent and of the form $D = A^{*}\sigma^{-m}\exp(\Delta Q/RT)$. The exponent m here is a function of both the GSI power law exponent n and the grain size sensitivity of the GSS flow equation.
3. Available experimentally calibrated m- and n-values for a range of metals, rocks and rock analogs (notably Magnox) predominantly lend support to the field boundary hypothesis as opposed to the Derby/Ashby and Shimizu models. Support also comes from the generally close correspondence of D–σ data for olivine and calcite with the GSS–GSI transition region in deformation mechanism maps drawn for these materials.
4. In view of the temperature dependence predicted in the recrystallized grain size versus stress models of Derby/Ashby, Shimizu and ourselves, and the observed dependence in some materials, temperature should be taken into careful account in recrystallized grain size paleo-piezometry. Existing piezometric relationships for various rocks are accordingly in need of revision via systematic exploration of the influence of temperature.
5. Grain size reduction by dynamic recrystallization is unlikely to result in a switch from GSI to GSS creep if grain growth is also operative. If the field boundary model holds, only minor rheological weakening is possible. The amount of weakening depends on the pure dislocation creep behavior (n-value) and on the relative contribution of GSI and GSS mechanisms to the overall steady state creep rate, at high strains. If both mechanisms contribute equally and n=3–4, the amount of weakening is expected to be <25%.
6. If grain growth is not inhibited, mechanisms other than grain size reduction by dynamic recrystalliza-

tion must be responsible for major rheological weakening and associated strain localization.

Acknowledgements The authors gratefully acknowledge discussions with Martyn Drury, Win Means, Ichiko Shimizu, Iona Stretton, and Stan White. We also thank Brian Evans and Greg Hirth for helpful reviews.

References

Ave Lallemant HG (1978) Experimental deformation of diopside and websterite. Tectonophysics 48:1–27

Braun J, Chéry J, Poliakov A, Mainprice D, Vauchez A, Tomassi A, Daignières M (1999) A simple parameterization of strain localization in the ductile regime. J Geophys Res (B) 104:25167–25181

Busch JP, Van der Pluijm BA (1995) Calcite textures, microstructures and rheological properties of marble mylonites in the Bancroft shear zone, Ontario, Canada. J Struct Geol 17:677–688

Carter NL, Horseman ST, Russell JE, Handin J (1993) Rheology of rocksalt. J Struct Geol 15:1257–1271

Cepeda LE, Rodriguez-Ibabe JM, Urcola JJ, Fuentes M (1989) Influence of dynamic recrystallisation on hot ductility of aluminium killed mild steel. Mater Sci Technol 5:1191–1199

Chopra PN, Paterson MS (1981) The experimental deformation of dunite. Tectonophysics 78:453–473

Chopra PN, Paterson MS (1984) The role of water in the deformation of dunite. J Geophys Res (B) 89:7861–7876

Chopra PN, Olgaard DL, Paterson MS (1988) High temperature flow of Carrara marble: revisited. EOS Trans Am Geophys Union 69:1417

Christie JM, Ord A, Koch PS (1980) Relationship between recrystallized grain size and flow stress in experimentally deformed quartzite. EOS Trans Am Geophys Union 61(17):377

Cox SF, Etheridge MA, Hobbs BE (1981) The experimental ductile deformation of polycrystalline and single crystal pyrite. Econ Geol 76:2105–2117

Cropper DR, Pask JA (1973) Creep of lithium fluoride single crystals at elevated temperatures. Philos Mag 27:1105–1124

De Bresser JHP (1996) Influence of pressure on the high temperature flow of Carrara marble. EOS Trans Am Geophys Union 77(46):F710

De Bresser JHP, Peach CJ, Reijs JPJ, Spiers CJ (1998) On dynamic recrystallization during solid state flow: effects of stress and temperature. Geophys Res Lett 25:3457–3460

Derby B (1990) Dynamic recrystallization and grain size. In: Barber DJ, Meredith PG (eds) Deformation processes in minerals, ceramics and rocks. Unwin Hyman, London, pp 354–364

Derby B, Ashby MF (1987) On dynamic recrystallization. Scripta Met 21:879–884

Drury MR, Urai JL (1990) Deformation-related recrystallization processes. Tectonophysics 172:235–253

Drury MR, Humphreys FJ, White SH (1985) Large strain deformation studies using polycrystalline magnesium as a rock analogue. Part II: dynamic recrystallization mechanisms at high temperatures. Phys Earth Planet Int 40:208–222

Durham WB, Goetze C (1977) Plastic flow of oriented single crystals of olivine. 1. Mechanical data. J Geophys Res 82:5737–5753

Edward GH, Etheridge MA, Hobbs BE (1982) On the stress dependence of sub-grain size. Text Microstruct 5:127–152

Etheridge MA, Wilkie JC (1979) Grain size reduction, grain boundary sliding and the flow strength of mylonites. Tectonophysics 58:159–178

Evans B, Kohlstedt DL (1995) Rheology of rocks. In: Ahrens TJ (ed.) Handbook of physical constants. Part 3 – rock physics and phase relations. Am Geophys Union, Washington, DC, pp 148–165

Fliervoet TF (1995) Deformation mechanisms in fine grained quartzo-feldspathic mylonites. Geol Ultraiectina 131. PhD Thesis, Utrecht University

Freeman B, Ferguson CC (1986) Deformation mechanism maps and micromechanics of rocks with distributed grain sizes. J Geophys Res 91(B):3849–3860

Friedman M, Higgs NG (1981) Calcite fabrics in experimental shear zones. Geophys Monograph Am Geophys Union 24:11–27

Fritzemeier L, Luton MJ, McQueen HJ (1980) Dislocation substructure in dynamic recovery and recrystallization of hot worked austenitic stainless steel. In: Haasen P, Gerold V, Kostorz G (eds) Strength of metals and alloys. Proc 5th Int Conf on the Strength of metals and alloys, Aachen. Pergamon, Toronto, pp 95–100

Frost HJ, Ashby MF (1982) Deformation mechanism maps. Pergamon Press, Toronto, pp 1–166

Furlong KP (1993) Thermal-rheological evolution of the upper mantle and the development of the San Andreas fault system. Tectonophysics 223:149–164

Glover G, Sellars CM (1973) Recovery and recrystallization during high temperature deformation of α-iron. Metall Trans 4:765–775

Govers R, Wortel MJR (1995) Extension of stable continental lithosphere and the initiation of lithosphere scale faults. Tectonics 14:1041–1055

Guillopé M, Poirier JP (1979) Dynamic recrystallization during creep of single-crystalline halite: an experimental study. J Geophys Res (B) 84:5557–5567

Hacker BR, Yin A, Christie JM, Snoke AW (1990) Differential stress, strain rate, and temperatures of mylonitization in the Ruby mountains, Nevada: implications for the rate and duration of uplift. J Geophys Res (B) 95:8569–8580

Hacker BR, Yin A, Christie JM, Davis GA (1992) Stress magnitude, strain rate and rheology of extended middle continental crust inferred from quartz grain sizes in the Whipple mountains, California. Tectonics 11:36–46

Handy MR (1989) Deformation regimes and the rheological evolution of fault zones in the lithosphere: the effects of pressure, temperature, grain size and time. Tectonophysics 163:119–152

Heilbronner R, Bruhn D (1998) The influence of three-dimensional grain size distributions on the rheology of polyphase rocks. J Struct Geol 20:695–705

Hippler SJ, Knipe RJ (1990) The evolution of cataclastic rocks from a pre-existing mylonite. In: Knipe RJ, Rutter EH (eds) Deformation mechanisms, rheology and tectonics. Geol Soc Lond Spec Publ 54:71–80

Hirth G, Tullis J (1992) Dislocation creep regimes in quartz aggregates. J Struct Geol 14:145–159

Hobbs BE, Muhlhaus HB, Ord A (1990) Instability, softening and localization of deformation. In: Knipe RJ, Rutter EH (eds) Deformation mechanisms, rheology and tectonics. Geol Soc Lond Spec Publ 54:143–166

Jacka TH, Li Jun (1994) The steady-state crystal size of deforming ice. Ann Glaciol 20:13–18

Jaroslow GE, Hirth G, Dick HJB (1996) Abyssal peridotite mylonites: implications for grain-size sensitive flow and strain localization in the oceanic lithosphere. Tectonophysics 256:17–37

Jin D, Karato S-I, Obata M (1998) Mechanisms of shear localization in the continental lithosphere; inferences from the deformation microstructures of peridotites from the Ivrea zone, northwestern Italy. J Struct Geol 20:195–209

Kameyama M, Yuen DA, Fujimoto H (1997) The interaction of viscous heating with grain-size dependent rheology in the formation of localized slip zones. Geophys Res Lett 24:2523–2526

Karato S-I, Toriumi M, Fujii T (1980) Dynamic recrystallization of olivine single crystals during high temperature creep. Geophys Res Lett 7:649–652
Karato S-I, Paterson MS, Fitz Gerald JD (1986) Rheology of synthetic olivine aggregates: influence of grain size and water. J Geophys Res (B) 91:8151–8176
Kirby SH, Raleigh CB (1973) Mechanisms of high-temperature, solid-state flow in minerals and ceramics and their bearing on the creep behavior of the mantle. Tectonophysics 19:165–194
Koch PS (1983) Rheology and microstructures of experimentally deformed quartz aggregates. PhD Thesis, Univ California, Los Angeles, pp 1–464
Kohlstedt DL, Weathers MS (1980) Deformation-induced microstructures, paleopiezometers, and differential stresses in deeply eroded fault zones. J Geophys Res (B) 85:6269–6285
Kronenberg AK, Tullis J (1984) Flow strengths of quartz aggregates: grain size and pressure effects due to hydrolitic weakening. J Geophys Res (B) 89:4281–4297
Luton MJ, Sellars CM (1969) Dynamic recrystallization in nickel and nickel–iron alloys during high temperature deformation. Acta Metall 17:1033–1044
Maruyama K, Karashima S, Oikawa H (1980) Analysis of steady-state creep of Fe–Mo alloys from the viewpoint of recovery. In: Haasen P, Gerold V, Kostorz G (eds) Strength of metals and alloys. Proc 5th Int Conf on Strength of metals and alloys, Aachen. Pergamon, Toronto, pp 283–288
McDonnell RD (1997) Deformation of fine-grained synthetic peridotite under wet conditions. Geol Ultraiectina 152. PhD Thesis, Utrecht University, pp 1–195
McDonnell RD, Peach CJ, Spiers CJ (1999) Flow behavior of fine-grained synthetic dunite in the presence of 0.5 wt% H2O. J Geophys Res (B) 104:17823–17845
McQueen, HJ, Baudelet B (1980) Comparison and contrast of mechanisms, microstructures, ductilities in superplasticity and dynamic recovery and dynamic recrystallization. In: Haasen P, Gerold V, Kostorz G (eds) Strength of metals and alloys. Proc 5th Int Conf on Strength of metals and alloys, Aachen. Pergamon, Toronto, pp 329–336
Means WD (1989) Synkinematic microscopy of transparent polycrystals. J Struct Geol 11:163–174
Mercier J-C, Anderson DA, Carter NL (1977) Stress in the lithosphere: Inferences from steady-state flow of rocks. Pageophysics 115:199–226
Nabarro FRN (1987) Theory of crystal dislocations. Dover, New York, pp 1–821
Newman J (1994) The influence of grain size and grain size distribution on methods for estimating paleostresses from twinning in carbonates. J Struct Geol 16:1589–1601
Newman J, Lamb WM, Drury MR, Vissers RLM (1999) Deformation processes in a peridotite shear zone: reaction-softening by a H_2O-deficient, continuous net transfer reaction. Tectonophysics 303:193–222
Ord A, Christie JM (1984) Flow stresses from microstructures in mylonite quartzites of the Moine thrust zone, Assynt area, Scotland. J Struct Geol 6:639–654
Orlova A, Pahutova P, Cadek J (1972) Dislocation structure and applied, effective and internal stress in high-temperature creep of alpha-iron. Philos Mag 25:865–877
Pahutova M, Orlova A, Kucharova K, Cadek J (1973) Steady-state creep in alpha iron as described in terms of effective stress and dislocation dynamics. Philos Mag 26:1099–1110
Parrish DK, Krivz AL, Carter NL (1976) Finite-element folds of similar geometry. Tectonophysics 32:183–207
Pfiffner OA (1982) Deformation mechanisms and flow regimes in limestones from the Helvetic zone of the Swiss Alps. J Struct Geol 4:429–442
Pieri M, Stretton I, Kunze K, Olgaard DL, Burg J-P (1998) Dynamic recrystallization in Carrara marble deformed in torsion to very high shear strains. Rheological and microstructural observations. EOS Trans Am Geophys Union 79(45):F851
Poirier JP (1980) Shear localization and shear instability in materials in the ductile field. J Struct Geol 2:135–142
Poirier JP (1985) Creep of crystals. Cambridge University Press, Cambridge, pp 1–260
Post RL (1977) High-temperature creep of Mt. Burnet dunite. Tectonophysics 42:75–110
Post A, Tullis J (1999) A recrystallized grain size piezometer for experimentally deformed feldspar aggregates. Tectonophysics 303:159–173
Ranalli (1984) Grain size distribution and flow stress in tectonites. J Struct Geol 6:443–447
Ross JV, Nielson KC (1978) High-temperature flow of wet polycrystalline enstatite. Tectonophysics 44:233–261
Ross JV, Avé Lallemant HG, Carter NL (1980) Stress dependence of recrystallized grain and subgrain size in olivine. Tectonophysics 70:39–61
Rutter EH (1995) Experimental study of the influence of stress, temperature and strain on the dynamic recrystallization of marble. J Geophys Res 100:24651–24663
Rutter EH (1999) On the relationship between the formation of shear zones and the form of the flow law for rocks undergoing dynamic recrystallization. Tectonophysics 303:147–158
Rutter EH, Brodie KH (1988) The role of tectonic grain size reduction in the rheological stratification of the lithosphere. Geol Rundsch 77:295–308
Sah JP, Richardson GJ, Sellars CM (1974) Grain-size effects during dynamic recrystallization of nickel. Metal Sci 8:325–331
Sakai T (1989) Dynamic recrystallization of metallic materials. In: Karato S-I, Toriumi M (eds) Rheology of solids and of the Earth. Oxford University Press, Oxford, pp 284–307
Schmid SM (1982) Laboratory experiments on the rheology and deformation mechanisms in calcite rocks and their applications to studies in the field. Mitteilungen Geol Inst ETH Univ Zürich, no 241, pp 1–62
Schmid SM, Paterson MS, Boland JN (1980) High temperature flow and dynamic recrystallization in Carrara marble. Tectonophysics 65:245–280
Shigematsu N (1999) Dynamic recrystallization in deformed plagioclase during progressive shear deformation. Tectonophysics 305:437–452
Shimizu I (1998) Stress and temperature dependence of recrystallized grain size: a subgrain misorientation model. Geophys Res Lett 25:4237–4240
Shimizu I (1999) A stochastic model of grain size distribution during dynamic recrystallization. Philos Mag (A) 79:1217–1231
Stretton IC, Olgaard DL (1997) A transition in deformation mechanism through dynamic recrystallization – evidence from high strain, high temperature torsion experiments. EOS Trans Am Geophys Union 78(46):F723
Streb G, Reppich B (1973) Steady state deformation and dislocation structure of pure and Mg-doped LiF single crystals. Phys Status Solidi 16:493–505
Takeuchi S, Argon SA (1976) Steady-state creep of single-phase crystalline matter at high temperature. J Mater Sci 11:1542–1566
Tullis J, Yund RA (1985) Dynamic recrystallization of feldspar: a mechanism for ductile shear zone formation. Geology 13:238–241
Tullis J, Dell'Angelo L, Yund RA (1990) Ductile shear zones from brittle precursors in feldspathic rocks: the role of dynamic recrystallization. Geophys Monograph Am Geophys Union 56:67–81
Tungatt PD, Humphreys FJ (1984) The plastic deformation and dynamic recrystallization of polycrystalline sodium nitrate. Acta Metall 32:1625–1635
Twiss RJ (1977) Theory and applicability of a recrystallized grain size paleopiezometer. Pageophysics 115:227–244
Twiss RF, Sellars CM (1978) Limits of applicability of the recrystallized grain size geopiezometer. Geophys Res Lett 5:337–340

Urai JL, Means WD, Lister GS (1986) Dynamic recrystallization of minerals. Geophys Monograph Am Geophys Union 36:161–199

Van der Wal D (1993) Deformation Processes in mantle peridotites. Geol Ultraiectina 102. PhD Thesis, Utrecht University, pp 1–180

Van der Wal D, Chopra PN, Drury MR, Fitz Gerald JD (1993) Relationships between dynamically recrystallized grain size and deformation conditions in experimentally deformed olivine rocks. Geophys Res Lett 20:1479–1482

Vissers RLM, Drury MR, Hoogerduijn Strating EH, Spiers CJ, Van der Wal D (1995) Mantle shear zones and their effect on lithosphere strength during continental breakup. Tectonophysics 249:155–171

Walker AN, Rutter EH, Brodie KH (1990) Experimental study of grain-size sensitive flow of synthetic hot-pressed calcite rock. In: Knipe RJ, Rutter EH (eds) Deformation mechanisms, rheology and tectonics. Geol Soc Lond Spec Publ 54:259–284

White SH (1979) Grain and sub-grain size variations across a mylonite zone. Contrib Mineral Petrol 70:193–202

White SH, Burrows SE, Carreras J, Shaw ND, Humphreys FJ (1980) On mylonites in ductile shear zones. J Struct Geol 2:175–187

Wolfenstine J, Shih J-H (1994) Creep behaviour and dislocation substructure evolution in the KBr–KI system. J Mater Sci 29:6199–6206

Young CM, Sherby OD (1973) Subgrain formation and subgrain-boundary strengthening in iron-based materials. J Iron Steel Inst 211:640–647

Zeuch DH (1983) On the inter-relationship between grain size sensitive creep and dynamic recrystallization of olivine. Tectonophysics 93:151–168